# EXPLORATION OF EMISSION SPECTRA FROM HIGHLY CHARGED TUNGSTEN IMPURITY IONS IN X-RAY WAVELENGTH RANGE OF 3.7–4.0 Å IN THE LARGE HELICAL DEVICE FOR FUSION PLASMA DIAGNOSTICS

### T. OISHI

Department of Quantum Science and Energy Engineering, Tohoku University

Sendai, Japan

Email: tetsutarou.oishi.a4@tohoku.ac.jp

<sup>1</sup>R. NISHIMURA, <sup>2,3</sup>S. MORITA, <sup>2,3</sup>M. GOTO, <sup>2,3</sup>Y. KAWAMOTO, <sup>4</sup>T. KAWATE, <sup>2,3</sup>I. MURAKAMI,

<sup>2,5</sup>D. KATO, <sup>2</sup>H.A. SAKAUE, <sup>1</sup>H. TAKAHASHI, <sup>1</sup>K. TOBITA

<sup>1</sup>Department of Quantum Science and Energy Engineering, Tohoku University

Sendai, Japan

<sup>2</sup>National Institute for Fusion Science, National Institutes of Natural Sciences

Toki, Japan

<sup>3</sup>Graduate Institute for Advanced Studies, SOKENDAI

Toki, Japan

<sup>4</sup>Naka Institute for Fusion Science and Technology, National Institutes for Quantum Science and Technology, Naka, Japan

<sup>5</sup>Interdisciplinary Graduate School of Engineering Sciences, Kyushu University

Fukuoka, Japan

### **Abstract**

The emission spectra of highly charged tungsten ions distributed in plasmas with central electron temperatures of about 4 keV in the Large Helical Device (LHD) have been investigated using X-ray crystal spectroscopy. As a result, emission lines from  $W^{42+}$  to  $W^{47+}$  were observed in the 3.7–4.0 Å wavelength range. The X-ray measurements demonstrate the feasibility of simultaneously determining tungsten impurity emission intensity, ion temperature, and electron temperature. Spectral data in this charge-state region are useful for diagnostics of tungsten impurities in the edge plasma—from the last closed flux surface to the pedestal region—under ITER-relevant conditions.

### 1. INTRODUCTION

Tungsten (W) is a candidate material for plasma-facing components in ITER and future fusion reactors because of its high melting point and low sputtering yield [1-3]. However, there is a concern that tungsten ions with a large atomic number of Z = 74 will cause large energy loss by radiation and ionization when the plasma is contaminated by the tungsten impurity. Therefore, it is important to understand and control tungsten impurity transport in high temperature plasmas for establishing reliable operation scenarios for fusion reactors. Spectroscopic studies for emissions released from tungsten ions in a combination with a tungsten pellet injection technique have been intensively conducted in the Large Helical Device (LHD) for contribution to the tungsten transport study in tungsten divertor fusion devices represented by ITER and for the expansion of the experimental database of tungsten line emissions. Simultaneous measurement of multiple charge states ranging from W<sup>0</sup> to W<sup>46+</sup> has been successfully conducted in LHD in the visible light, vacuum ultraviolet (VUV), extreme ultraviolet (EUV), and X-ray wavelength regions [4,5]. Since the dominant charge states of these depend on the electron temperature, the electron temperature can be controlled and the charge distribution is varied by adjusting the power and timing of the plasma heating. At present, the electron temperature at the center of the plasma,  $T_{e0}$ , that can be achieved while sustaining significant tungsten ion content in the plasma is about 4 keV. In this electron temperature region, impurity ions emit strongly in the X-ray wavelength range, and the spectroscopic data will contribute to the monitoring of impurities in ITER-relevant edge plasmas. Therefore, in the present study, the X-ray spectra in LHD were carefully examined to explore the emission lines that are useful for the tungsten impurity diagnostics.

### 2. W PELLET INJECTION EXPERIMENT AND SPECTROSCOPIC DIAGNOSTICS IN LHD

LHD is a heliotron type plasma confinement device which has the major/minor radii of 3.6/0.64 m in the standard configuration with maximum plasma volume of  $30 \text{ m}^3$  and toroidal magnetic field of 3 T [6]. The coil system consists of a set of two continuous superconducting helical coils with poloidal pitch number of 2 and toroidal pitch number of 10 and three pairs of superconducting poloidal coils. Figure 1(a) illustrates the top view of shape of plasma in LHD device with the position of the magnetic axis in the major radius,  $R_{ax}$ , of 3.6m together

with schematic drawings of neutral beam injection (NBI) for heating, spectroscopic diagnostics, and impurity pellet injection. The red dashed arrows indicate the optical axes of the spectroscopic diagnostics, which are shown for the X-ray crystal spectrometer (XCS) [7] and the EUV spectrometers (denoted as "EUV Short" [8], "EUV Long" [9], "EUV Short2" [10], and "EUV Long2" [11]). Figure 1(b) illustrates vertical observation range of "EUV Short" and "EUV Long" with cross sections of the magnetic surfaces including the optical axes of the respective spectrometers. Observation ranges of the space-resolved spectrometers "EUV Short2" and "EUV Long2" are also illustrated in Fig. 1(c). Tungsten ions are distributed in the NBI-heated LHD plasma by injecting a pellet consisting of a small piece of tungsten metal wire enclosed by a carbon or polyethylene pellet with a shape of a cylindrical tube [12].

### 3. X-RAY SPECTROSCOPY OF TUNGSTEN IMPURITY IONS IN LHD

### 3.1. Newly observed W<sup>42+</sup>–W<sup>47+</sup> X-ray spectra in 3.7–4.0 Å

Figure 2(a) shows the spectra of tungsten ions measured by XCS during the time period when  $T_{e0}$  was around 4 keV. Since the wavelength range that can be measured per discharge is limited, the spectra measured at different wavelength ranges during 10 discharges were merged to cover the 3.7-4.0 Å wavelength range. The working gas of the plasma discharge was hydrogen, the magnetic axis position,  $R_{ax}$ , was 3.6 m, and the toroidal magnetic field,  $B_t$ , was 2.75 T in the counterclockwise direction viewed from the top. Tungsten ions were distributed in the LHD plasma by injecting a pellet consisting of a small piece of tungsten metal wire, equivalent to  $3.5 \times 10^{17}$  tungsten atoms, enclosed in a carbon tube. For identification of the observed lines, we calculated the emission spectra from W<sup>42+</sup> to W<sup>47+</sup>, of which the fractional abundance is large at around  $T_{e0} = 4$  keV, using an atomic structure calculation code Flexible Atomic Code (FAC) [13] combined with a collisional-radiative (CR) model. For each charge state, energy levels and rate coefficients for elementary atomic processes were calculated, and the spectra were synthesized using the CR model under an electron temperature of 4 keV and an electron density of  $2 \times 10^{13}$  cm<sup>-3</sup>. The resulting spectra were then weighted by the fractional abundance ratios calculated from the ionization and recombination rate coefficients in the ADAS database, and are shown in Fig. 2(b). The

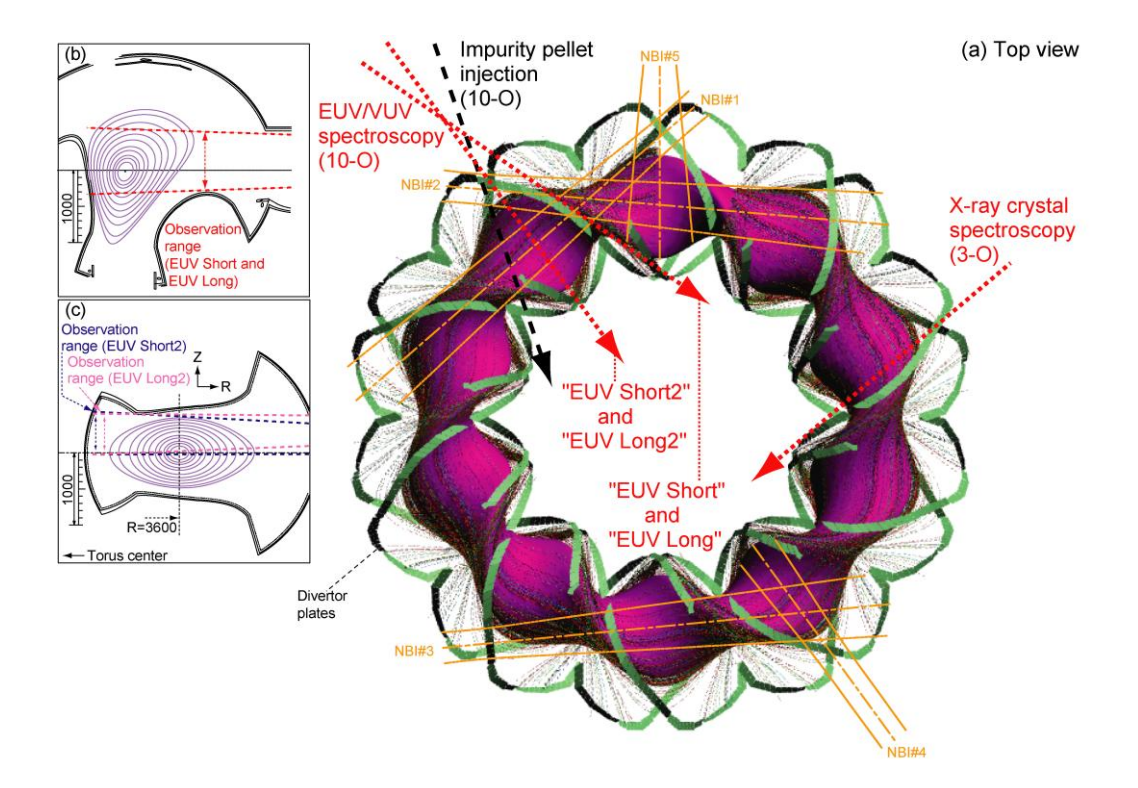


FIG. 1. (a) Top view of shape of plasma in LHD device ( $R_{ax} = 3.6 \text{ m}$ ) together with schematic drawings of neutral beam injection (NBI) for heating, spectroscopic diagnostics, and impurity pellet injection. The light blue dashed arrows indicate the optical axes of the spectroscopic diagnostics, which are shown for the X-ray crystal spectrometer, the EUV spectrometers 'EUV Short', 'EUV Long', 'EUV Short2', and 'EUV Long2'. (b) Vertical observation range of 'EUV Short' and 'EUV Long' is illustrated with cross sections of the magnetic surfaces including the optical axes of the respective spectrometers. Observation ranges of the space-resolved spectrometers (c) 'EUV Long2' and 'EUV Short2' are also illustrated.

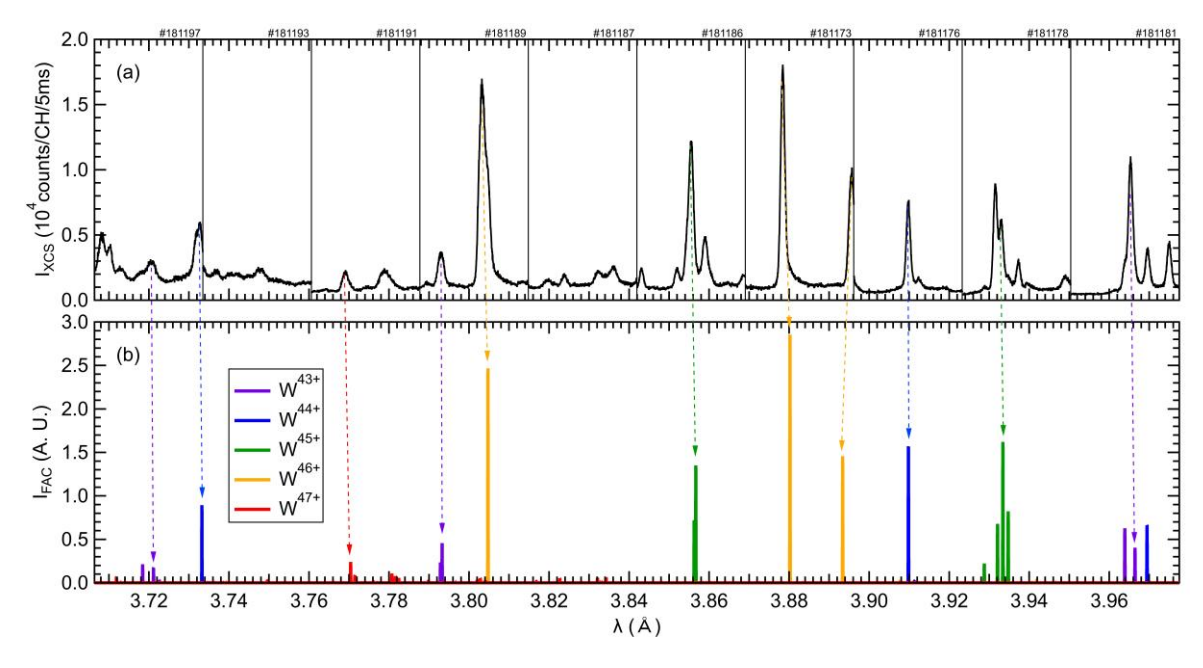


FIG. 2. X-ray spectra including the emission lines ranging  $W^{43+}$ — $W^{47+}$ , comparing (a) the spectra observed at LHD and (b) the spectra calculated by the flexible atomic code (FAC).

wavelengths of the emission lines with strong intensity are compared with the measured and calculated values, and are shown together with the corresponding charge states in Table 1. The observed and calculated wavelengths are in good agreement, and these lines are expected to be useful for monitoring ions in each charge state. The emission line observed at 3.7691 Å is estimated to have a valence of  $W^{47+}$  and a transition of  $(3p^63d^9-3p^63d^86f)$ . This extends the charged region previously observed in LHD and serves as a diagnostic tool for higher electron temperatures.

## 3.2. Monitoring of tungsten impurity behavior via simultaneous measurement of multiple charge states

Simultaneous measurements across a broad band enable monitoring of tungsten impurities in diverse charge states. The observation of  $W^{47+}$  has extended the upper limit of the charge range previously measured simultaneously. Figure 3 shows (a) X-ray wavelength spectrum at

Table 1. Wavelengths of tungsten emission lines observed using XCS,  $\lambda_{XCS}$ , and calculated with FAC,  $\lambda_{FAC}$ , together with the charge states.

λxcs (Å)	λfac (Å)	Ion
3.7204	3.7212	$W^{43+}$
3.7323	3.7332	$W^{44+}$
3.7691	3.7704	$W^{47+}$
3.7930	3.7933	$W^{43+}$
3.8033	3.8048	$W^{46+}$
3.8555	3.8567	$W^{45+}$
3.8784	3.8803	$W^{46+}$
3.8956	3.8933	$W^{46+}$
3.9098	3.9098	$W^{44+}$
3.9330	3.9334	$W^{45+}$
3.9655	3.9664	$W^{43+}$
3.9694	3.9694	$W^{44+}$

3.758–3.798 Å and (b) 5–60 Å and (c) 100–150 Å EUV wavelength spectrum when the W<sup>47+</sup> emission line was observed. Two cases are shown:  $T_{e0} = 2.3$  keV (blue) and  $T_{e0} = 4.0$  keV (red). The W<sup>47+</sup> 3.7691 Å emission line was observed in the X-ray region, while its neighbouring charge states W<sup>41+</sup> to W<sup>46+</sup> were observed in the EUV region. Figure 4 shows temporal evolution of (a) heating power of ECH and NBI, (b)  $T_{e0}$  and  $n_e$ , emission intensities of (c) UTA spectra consisting of the charge range from W<sup>27+</sup> to W<sup>42+</sup>, (d) line spectra from W<sup>41+</sup> to W<sup>45+</sup>, (e) W<sup>46+</sup>, and (e) W<sup>47+</sup>. Panels (c-e) and (f) are obtained in the EUV and X-ray wavelength ranges, respectively. In this discharge,  $T_{e0}$  initially decreases to 1.7 keV after pellet injection and then increases to 5.0 keV. When  $T_{e0} < 3$  keV, the UTA at 45-55 Å of W<sup>27+</sup>–W<sup>42+</sup> serves as an indicator of tungsten impurities. After t = 4.5 s, the UTA intensity decreases, and the W<sup>41+</sup>–W<sup>47+</sup> emission lines appear sequentially. At t = 4.9 s, W<sup>47+</sup> exhibits a maximum at  $T_{e0} = 4.3$  keV, indicating its usefulness as an indicator of tungsten impurities in the electron temperature region around 4 keV.

### 3.3. Ion temperature measurement using Doppler broadening of a W<sup>46+</sup> line

X-ray spectroscopy enables precise observation of spectral shapes due to its high wavelength dispersion, and it is also possible to derive ion temperature from the line width. Figure 5 shows radial profiles of fundamental plasma parameters and intensity of highly charged W ion emission in a plasma with  $T_{\rm e0}$  of approximately 4 keV: (a) Electron temperature,  $T_{\rm e}$ , and electron density,  $n_{\rm e}$ , measured by Thomson scattering, and ion temperature,  $T_{\rm i}$ , measured by a charge exchange recombination spectroscopy (CXRS), versus effective minor radius,  $r_{\rm eff}$ , and (b)

W<sup>46+</sup> measured by the "EUV Short2" spectrometer and W<sup>41+</sup>, W<sup>42+</sup>, W<sup>43+</sup>, and W<sup>45+</sup> measured by the "EUV Long2" spectrometer. The W ion emission intensity is the line-of-sight integral, thus, the horizontal axis in the figure 5(b) is the minimum effective radius,  $r_{\rm eff,min}$  along each line of sight. Since W<sup>46+</sup> is localized in the plasma core in LHD, Doppler broadening in the W<sup>46+</sup> spectrum reflects  $T_i$  in the plasma core. Figure 6(a) shows an X-ray spectrum of W<sup>46+</sup> at 3.8784Å and derivation of ion temperature via Gaussian fitting. A Gaussian function with the full width of half maximum (FWHM)  $8.3 \times 10^{-4}$  Å was used as the instrumental function,  $\Delta \lambda_{\rm Ins}$ . As indicated by the red circle in Fig. 6(b), the optimal value of  $\Delta \lambda_{\rm Ins}$  was determined such that the ion temperature,  $T_i$  w<sup>46+</sup>, derived from the Doppler broadening of W<sup>46+</sup> matches the plasma-center ion temperature,  $T_i$  c<sup>6+</sup>, obtained via CXRS. The green square and blue triangle indicate the extent to which  $T_i$  w<sup>46+</sup> is overestimated or underestimated when  $\Delta \lambda_{\rm Ins}$  was intentionally set to values smaller and larger than the optimal value, respectively. As shown here, accurate evaluation of  $\Delta \lambda_{\rm Ins}$  is extremely important in  $T_i$  measurement using Doppler broadening of W<sup>46+</sup>. Figure 7 shows electron density dependence of W<sup>46+</sup> ion temperature,  $T_i$  w<sup>46+</sup>, and comparison with and without p-NBI injection for ion heating. In discharges where p-NBIs are injected,  $T_i$  w<sup>46+</sup> is approximately 0.2 to 0.3 keV higher compared to discharges without p-NBIs, exhibiting behavior consistent with the amount of ion heating power.

### 3.4. Electron temperature measurement using a $W^{46+}$ line intensity ratio

It is known that by selecting two appropriate line spectra from the wavelength spectrum data obtained through plasma spectroscopic measurement, their intensity ratio may exhibit dependence on plasma parameters such as  $n_e$  or  $T_e$ . Figure 8 shows temporal evolution of (a) heating power of ECH and NBI, (b)  $T_{e0}$  and  $n_e$ , emission intensities of (c) UTA spectra consisting of the charge range from W<sup>27+</sup> to W<sup>42+</sup>, (d) W<sup>46+</sup> 3.8784 Å (3 $p^6$ 3 $d^{10}$  – 3 $p^6$ 3 $d^9$ 6f) and 3.8956 Å (3 $p^6$ 3 $d^{10}$  – 3 $p^5$ 3 $d^{10}$ 5d0 lines, and (f) line intensity ratio between the two W<sup>46+</sup> lines. As

 $T_{\rm e}$  increases, the line intensity ratio between W<sup>46+</sup> 3.8784 Å and 3.8956 Å decreases. Figure 9 shows  $T_{\rm e}$  dependence of the line intensity ratio. FAC calculations reproduce the observed  $T_{\rm e}$  dependence of the line intensity

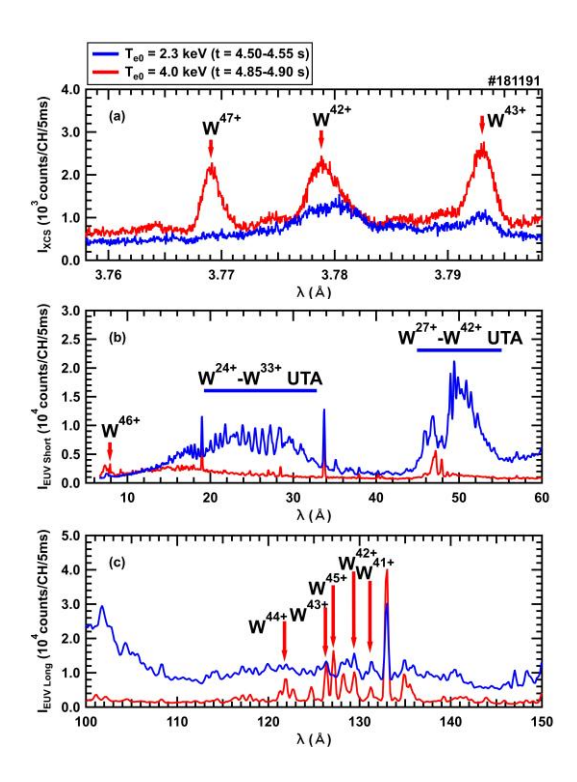


FIG. 3. (a) X-ray wavelength spectrum at 3.758–3.798 Å and (b) 5–60 Å and (c) 100–150 Å EUV wavelength spectrum when the W<sup>47+</sup> emission line was observed. The figures show cases for central electron temperatures, T<sub>e0</sub>, = 2.3 keV (blue) and 4.0 keV (red). The W<sup>47+</sup> 3.7691 Å emission line was observed in the X-ray region, while its neighbouring charge states W<sup>41+</sup> to W<sup>46+</sup> were observed in the EUV region.

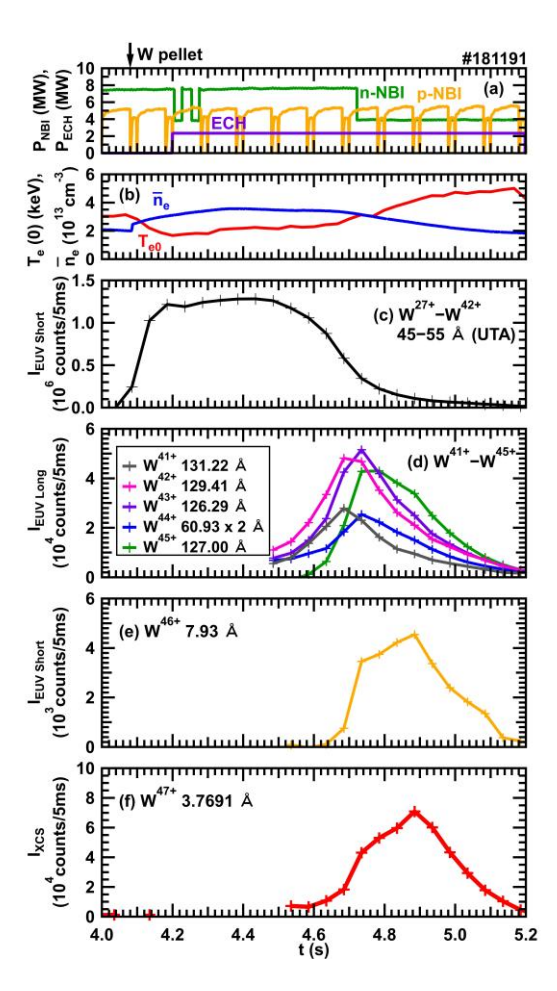


FIG. 4. Temporal evolution of (a) heating power of ECH and NBI, (b)  $T_{e0}$  and  $n_e$ , emission intensities of (c) UTA spectra consisting of the charge range from  $W^{27+}$  to  $W^{42+}$ , (d) line spectra from  $W^{41+}$  to  $W^{45+}$ , (e)  $W^{46+}$ , and (e)  $W^{47+}$ . (c-e) and (f) are observed in the EUV and X ray wavelength ranges, respectively.

ratio. In the electron density range over  $n_{\rm e} = 10^9 - 10^{15}$  cm<sup>-3</sup>, negligible density dependence of the line intensity ratio is exhibited, as confirmed by the FAC calculations. Therefore, the W<sup>46+</sup> 3.8784 Å / 3.8956 Å ratio was found to be useful for  $T_{\rm e}$  measurements.

### 4. SUMMARY

Spectroscopic measurements of tungsten ions have been conducted in the Large Helical Device (LHD) using tungsten pellets to investigate high-Z impurity transport in fusion plasmas and to expand the spectral database. Numerous emission lines with  $W^{42+}$ — $W^{47+}$  are newly observed in the X-ray wavelength range of 3.7–4.0 Å.  $W^{47+}$  3.7691 Å represents a new charge state region for the LHD experiment. The feasibility of simultaneously determining the W emission intensity, ion temperature,  $T_{\rm i}$ , and electron temperature,  $T_{\rm e}$ , has been demonstrated as follows: (1)  $W^{47+}$  serves as an indicator of tungsten impurities in the electron temperature region around 4

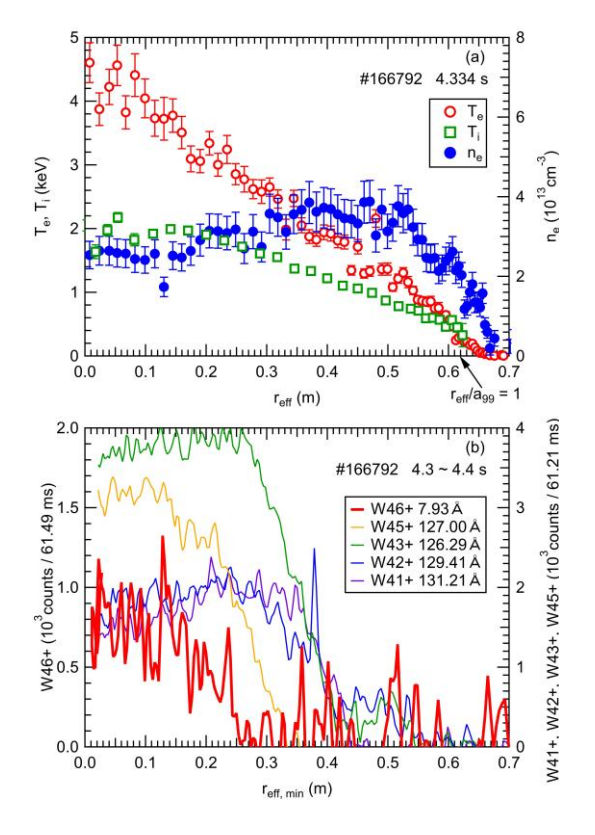


FIG. 5. Radial profiles of fundamental plasma parameters and intensity of highly charged W ion emission in a plasma with Te0 of approximately 4 keV. (a) Electron temperature, Te, and electron density, ne, measured by Thomson scattering, and ion temperature, Ti, measured by a charge exchange recombination spectroscopy, versus effective minor radius, reff. (b) W<sup>46+</sup> measured by the 'EUV Short2' spectrometer and W<sup>41+</sup>, W<sup>42+</sup>, W<sup>43+</sup>, and W<sup>45+</sup> measured by the 'EUV Long2' spectrometer. The W ion emission intensity is the line-of-sight integral. The horizontal axis in the figure 5(b) is the minimum effective radius, reff.min along each line of sight.

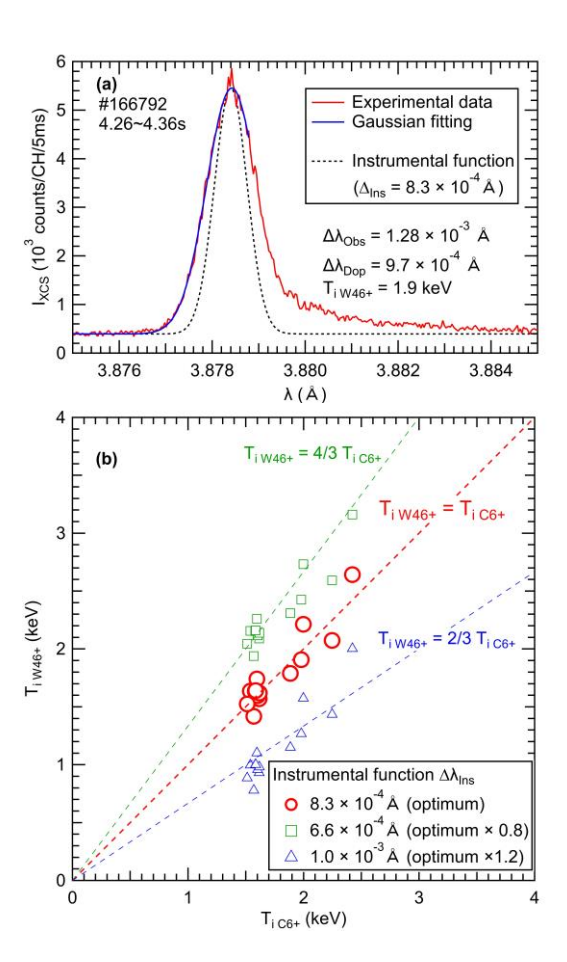


FIG. 6. (a) X-ray spectrum of W<sup>46+</sup> at 3.8784Å and derivation of ion temperature via Gaussian fitting. A Gaussian function with FWHM 8.3 × 10<sup>-4</sup> Å was used as the instrumental function. (b) As indicated by the red circle, the optimal width of the instrumental function was determined such that the ion temperature, T<sub>i</sub> w<sup>46+</sup>, derived from the Doppler broadening of W<sup>46+</sup> matches the plasma-center ion temperature, T<sub>i</sub> c<sup>6+</sup>, obtained via charge-exchange recombination spectroscopy. The green square and blue triangle show T<sub>i</sub> w<sup>46+</sup> values derived when the instrumental function was intentionally set to values smaller and larger than the optimal value, respectively.

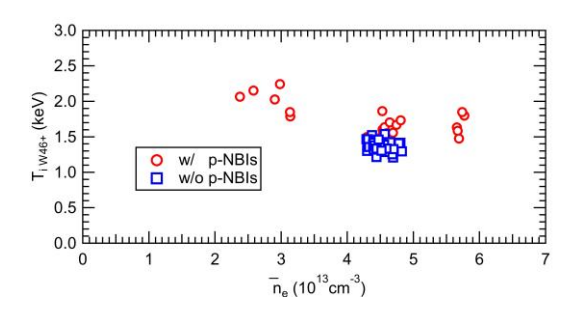


FIG. 7. Electron density dependence of  $W^{46+}$  ion temperature,  $T_i w^{46+}$ , and comparison with and without p-NBI injection.

keV. (2) In  $T_i$  measurement using Doppler broadening of W<sup>46+</sup> 3.8784 Å, accurate evaluation of the instrument function,  $\Delta \lambda_{\text{Ins}}$ , is critical. (3) W<sup>46+</sup> 3.8784 Å / 3.8956 Å intensity ratio provides a practical  $T_e$  diagnostics.

### **ACKNOWLEDGEMENTS**

The authors thank all the members of the LHD team for their cooperation with the LHD operation. This work was partially supported by JSPS KAKENHI (Grant Numbers JP20K03896, JP21H04460, and JP23H00127), the NIFS Collaboration Research program (Grant Numbers NIFS23KIPP031 and NIFS23KIPF007). The data supporting the findings of this study are available in the LHD experiment data repository at https://doi.org/10.57451/lhd.analyzed-data.

### REFERENCES

- [1] ITER Physics Basis Editors, ITER Physics Expert Group Chairs and Co-Chairs, ITER Joint Central Team and Physics Integration Unit, Chapter 1: Overview and summary, Nucl. Fusion **39** (1999) 2137–2174.
- [2] Neu, R., Dux, R., Kallenbach, A. *et al.*, Tungsten: An option for divertor and main chamber plasma facing components in future fusion devices, Nucl. Fusion **45** (2005) 209–218.
- [3] Roth, J., Tsitrone, E., Loarer, T. *et al.*, Tritium inventory in ITER plasma-facing materials and tritium removal procedures, Plasma Phys. Control. Fusion **50** (2008) 103001.
- [4] Oishi, T., Morita, S., Kato, D. *et al.*, Observation of tungsten emission spectra up to W<sup>46+</sup> ions in the Large Helical Device and contribution to the study of high-Z impurity transport in fusion plasmas Nucl. Fusion **64** (2024) 106011.

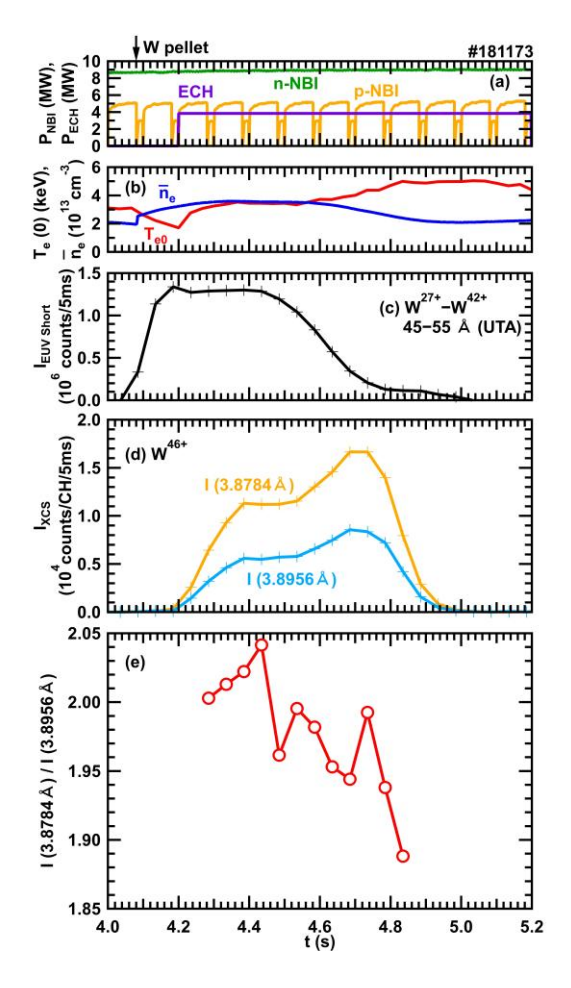


FIG. 8. Temporal evolution of (a) heating power of ECH and NBI, (b)  $T_{e0}$  and  $n_e$ , emission intensities of (c) UTA spectra consisting of the charge range from  $W^{27+}$  to  $W^{42+}$ , (d)  $W^{46+}$  3.8784 Å and 3.8956 Å lines, and (f) line intensity ratio between the two  $W^{46+}$  lines.

- [5] Morita, S., Oishi, T., Zhang, L. *et al.*, Recent Progress on Atomic Spectroscopy of Highly Ionized Ions in Laboratory Plasmas for Fusion Research Journal of Atomic, Molecular, Condensed Matter and Nano Physics **10** (2023) 39–51.
- [6] Ida, K, Yoshinuma, M., Kobayashi, M. *et al.*, Overview of Large Helical Device experiments of basic plasma physics for solving crucial issues in reaching burning plasma conditions, Nucl. Fusion **64** (2024) 112009.
- [7] Morita, S. and Goto, M., X-ray crystal spectrometer with a charge-coupled-device detector for ion temperature measurements in the large helical device, Rev. Sci. Instrum. **74** (2003) 2375–2387.
- [8] Chowdhuri M.B., Morita S. and Goto M., Characteristics of an absolutely calibrated flat-field extreme ultraviolet spectrometer in the 10–130 Å range for fusion plasma diagnostics, Appl. Opt. **47** (2008) 135–146.
- [9] Chowdhuri M.B., Morita S., Goto M. *et al.*, Spectroscopic comparison between 1200 grooves/mm ruled and

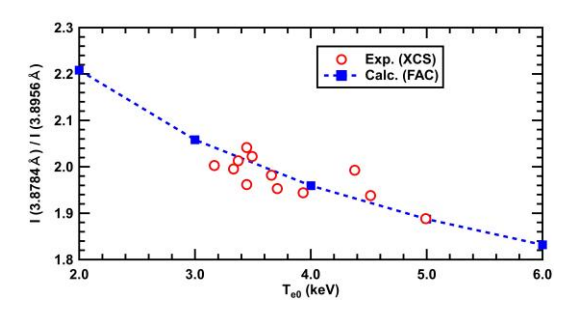


FIG. 9.  $T_e$  dependence of the line intensity ratio between  $W^{46+}$  3.8784 Å and 3.8956 Å. FAC calculations reproduce the observed  $T_e$  dependence of the line intensity ratio.

### T. OISHI et al., conference preprint

- holographic gratings of a flat-field spectrometer and its absolute sensitivity calibration using bremsstrahlung continuum, Rev. Sci. Instrum. **78** (2007) 23501.
- [10] Huang, X. L., Morita, S., Oishi, T. *et al.*, Space-resolved extreme ultraviolet spectroscopy free of high-energy neutral particle noise in wavelength range of 10–130 Å on the large helical device, Rev. Sci. Instrum. **85** (2014) 043511.
- [11] Zhang H.M., Morita S., Oishi T. *et al.*, Performance improvement of two-dimensional EUV spectroscopy based on high-frame-rate CCD and signal normalization method in large helical device, Jpn. J. Appl. Phys. **54** (2015) 086101.
- [12] Huang, X. L., Morita, S., Oishi, T. *et al.*, Coaxial pellets for metallic impurity injection on the large helical device, Rev. Sci. Instrum. **85** (2014) E811–E818.
- [13] Gu, M.F., Indirect X-Ray Line-Formation Processes in Iron L-Shell Ions, Astrophysical Journal 582 (2003) 1241.